

The Scale-Invariant Scotogenic Model

Amine Ahriche,^{1,2,i} Kristian L. McDonald^{3,ii} and Salah Nasri^{4,5,iii}

¹ *Department of Physics, University of Jijel, PB 98 Ouled Aissa, DZ-18000 Jijel, Algeria*

² *The Abdus Salam International Centre for Theoretical Physics, Strada Costiera 11, I-34014, Trieste, Italy*

³ *ARC Centre of Excellence for Particle Physics at the Terascale, School of Physics, The University of Sydney, NSW 2006, Australia*

⁴ *Physics Department, UAE University, POB 17551, Al Ain, United Arab Emirates*

Abstract

We investigate a minimal scale-invariant implementation of the scotogenic model and show that viable electroweak symmetry breaking can occur while simultaneously generating one-loop neutrino masses and the dark matter relic abundance. The model predicts the existence of a singlet scalar (dilaton) that plays the dual roles of triggering electroweak symmetry breaking and sourcing lepton number violation. Important constraints are studied, including those from lepton flavor violating effects and dark matter direct-detection experiments. The latter turn out to be somewhat severe, already excluding large regions of parameter space. None the less, viable regions of parameter space are found, corresponding to dark matter masses below (roughly) 10 GeV and above 200 GeV.

ⁱaahriche@ictp.it

ⁱⁱkristian.mcdonald@sydney.edu.au

ⁱⁱⁱsnasri@uaeu.ac.ae

1 Introduction

The discovery of the Higgs boson provides an explanation for the origin of mass in the charged fermion and gauge sectors of the Standard Model (SM). However, despite this great success, a number of problems remain. In particular, our understanding of the origin of neutrino mass is incomplete, and we do not know the constituent properties of the dark matter (DM) that appears necessary on galactic scales. In addition to these puzzles, the origin of the $\mathcal{O}(100)$ GeV mass-parameter that determines the weak scale in the SM also remains a mystery. Thus, with regard to the mechanisms of mass in the universe, there remains much to be discovered.

The scotogenic model is a simple framework that aims to address some of these shortcomings [1]. It offers an explanation for the origin of neutrino mass and the nature of DM by proposing a common or unified solution to these puzzles. In this approach, neutrinos acquire mass as a radiative effect, at the one-loop level, due to interactions with a Z_2 -odd sector that includes DM candidates. The resulting theory gives a simple model for neutrino mass and DM, and has been well-studied in the literature [2].

Motivated by the simplicity of the scotogenic model, and our inadequate understanding of the origin of the weak scale, in this work we investigate a minimal scale-invariant (SI) implementation of the scotogenic model (hereafter, the SI scotogenic model). Our goal is to maintain the appealing features of the scotogenic model, namely the explanation for both neutrino mass and DM, while incorporating a dynamical model for the origin of the weak scale. In such a model, the dimensionful parameters, including the Higgs mass, are born as a dynamical effect via radiative symmetry breaking [3]. Due to their common origin, both the Higgs mass and the exotic masses should appear at a similar scale, of $\mathcal{O}(\text{TeV})$, enhancing the prospects for testing the model. The resulting theory provides a common framework for the aforementioned problems relating to mass - namely the origin of neutrino mass, the origin of the weak scale, and the nature of DM.

We investigate the SI scotogenic model in detail, demonstrating that viable electroweak symmetry breaking can be achieved, while simultaneously generating neutrino masses and the DM relic abundance. The model predicts a singlet scalar (dilaton) that plays two important roles - it triggers electroweak symmetry breaking and sources the lepton number violation that allows radiative neutrino mass. Important constraints are studied, including those from lepton flavor violating effects, DM direct-detection experiments, and the Higgs sector, such as the invisible Higgs decay width and Higgs-dilaton mixing. Direct-detection constraints turn out to be rather severe and we find that large regions of parameter space are already excluded. None the less, viable parameter space is found with a DM mass below (roughly) 10 GeV or above 200 GeV. The model can be experimentally probed in a number of ways, including: $\mu \rightarrow e + \gamma$ searches, future direct-detection experiments, precision studies of the Higgs decays $h \rightarrow \gamma\gamma$ and $h \rightarrow \gamma Z$, and collider searches for an inert doublet.

Before proceeding we note that a number of earlier papers have studied relationships between neutrino mass and DM; see e.g. Refs. [4, 5, 6, 7], and also Ref. [8], in which DM stability follows from an accidental symmetry. Earlier works investigating SI extensions of

the SM appear in Ref. [9] and, in particular, studies of SI models for neutrino mass can be found in Refs. [10, 11].

The structure of this paper is as follows. In Section 2 we introduce the model and detail the symmetry breaking sector. We turn our attention to the origin of neutrino mass in Section 3 and discuss various constraints in Sections 4 and 5. Dark matter is discussed in Section 6 and our main analysis and results appear in Section 7. Conclusions are drawn in Section 8.

2 The Scale-Invariant Scotogenic Model

The minimal SI implementation of the scotogenic model is obtained by extending the SM to include three generations of gauge-singlet fermions, $N_{iR} \sim (1, 1, 0)$, where $i = 1, 2, 3$, labels generations, a second SM-like scalar doublet, $S \sim (1, 2, 1)$, and a singlet scalar $\phi \sim (1, 1, 0)$. A Z_2 symmetry with action $\{N_R, S\} \rightarrow -\{N_R, S\}$ is imposed on the model.¹ The scalar ϕ , as well as the SM fields, transform trivially under this symmetry. The lightest Z_2 -odd particle is stable and may be a DM candidate; this should be taken as either the lightest singlet fermion N_1 or a neutral component of the the doublet S , as discussed below. The scalar ϕ plays the dual roles of sourcing lepton number violation, to allow neutrino mass, and triggering electroweak symmetry breaking.

With this field content, the most-general Lagrangian consistent with both the SI and Z_2 symmetries contains the terms

$$\mathcal{L} \supset i\bar{N}_R\gamma^\mu\partial_\mu N_R + \frac{1}{2}(\partial^\mu\phi)^2 + |D^\mu S|^2 - \frac{y_i}{2}\phi\overline{N_{iR}^c}N_{iR} - g_{i\alpha}\overline{N_{iR}}L_\alpha S - V(\phi, S, H), \quad (1)$$

where $L_\alpha \sim (1, 2, -1)$ denotes the SM lepton doublets, with generations labeled by Greek letters, $\alpha, \beta = e, \mu, \tau$. We denote the SM scalar doublet as $H \sim (1, 2, 1)$ and $V(\phi, S, H)$ is the most-general scalar potential consistent with the symmetries. The SI symmetry precludes any dimensionful parameters in the model, including bare Majorana mass terms for the fermions N_i .

2.1 Symmetry Breaking

In the absence of dimensionful parameters, the scalar potential contains only quartic interactions:

$$\begin{aligned} V(\phi, S, H) = & \lambda_H |H|^4 + \frac{\lambda_\phi}{4}\phi^4 + \frac{\lambda_S}{2}|S|^4 + \frac{\lambda_{\phi H}}{2}\phi^2|H|^2 + \frac{\lambda_{\phi S}}{2}\phi^2|S|^2 + \lambda_3|H|^2|S|^2 \\ & + \lambda_4|H^\dagger S|^2 + \frac{\lambda_5}{2}(S^\dagger H)^2 + \text{H.c.} \end{aligned} \quad (2)$$

where λ_5 can be taken real without loss of generality. The desired VEV pattern has $\langle S \rangle = 0$, to preserve the Z_2 symmetry, with $\langle H \rangle \neq 0$ and $\langle \phi \rangle \neq 0$, to break both the SI and electroweak

¹This model was also mentioned in Ref. [12].

symmetries. In addition to the doublet scalar S , we shall see that the spectrum contains an SM-like scalar h_1 and a dilaton h_2 .

Radiative corrections play an important role in triggering the desired symmetry breaking pattern. A full analysis of the potential requires the inclusion of leading-order loop corrections; however, in general, the full one-loop corrected potential is not analytically tractable. None the less, as discussed in Ref. [11] (and guided by Ref. [13]), simple analytic expressions can be obtained by noting the following. Loop corrections involving SM fields are dominated by top-quark loops, due to the large Yukawa coupling. To allow viable electroweak symmetry breaking and give a positively-valued dilaton mass, these corrections must be dominated by loop corrections from a beyond-SM scalar, namely S . Thus, loop corrections from S and t are expected to dominate and, to reasonable approximation, one can neglect loop corrections involving the light scalars (namely the SM-like Higgs and the dilaton). More precisely, this gives an approximation to the potential up to corrections of $\mathcal{O}(M_{h_1}^4/M_S^4)$ [11], which is reasonable provided one restricts attention to $M_S \gtrsim 200$ GeV.

Adopting this approximation, and writing the SM scalar in unitary gauge as $H = (0, h/\sqrt{2})$, the one-loop corrected potential for h and ϕ is

$$V_{1-l}(h, \phi) = \frac{\lambda_H}{4}h^4 + \frac{\lambda_{\phi H}}{4}\phi^2h^2 + \frac{\lambda_\phi}{4}\phi^4 + \sum_{i=\text{all fields}} n_i G(M_i^2(h, \phi)), \quad (3)$$

where n_i is a multiplicity factor, Λ is the renormalization scale, and the sum is over all fields barring the light scalars (h and ϕ) and the light SM fermions (all but the top-quark). The function G is given by

$$G(X) = \frac{X^2}{64\pi^2} \left[\log \frac{X}{\Lambda^2} - \frac{3}{2} \right]. \quad (4)$$

In the absence of bare dimensionful parameters, the field-dependent masses can be written as

$$M_i^2(h, \phi) = \frac{\alpha_i}{2}h^2 + \frac{\beta_i}{2}\phi^2, \quad (5)$$

where α_i and β_i are constants.

Symmetry breaking is triggered via dimensional transmutation, introducing a dimensionful parameter into the theory in exchange for one of the dimensionless couplings (which is now fixed in terms of the other parameters). Analyzing the potential reveals a minimum with both $\langle \phi \rangle \equiv x \neq 0$ and $\langle h \rangle \equiv v \neq 0$ for $\lambda_{\phi H} < 0$. If one considers the tree-level potential, the desired VEV pattern is triggered at the scale Λ where the running couplings obey $2\sqrt{\lambda_H(\Lambda)\lambda_\phi(\Lambda)} + \lambda_{\phi H}(\Lambda) = 0$. Including loop corrections, subject to our approximation, modifies this relation to

$$2 \left\{ \lambda_H \lambda_\phi + \frac{\lambda_H}{x^2} \sum_i n_i \left\{ \beta_i - \alpha_i \frac{v^2}{x^2} \right\} G'(M_i^2) \right\}^{1/2} + \lambda_{\phi H} + \frac{2}{x^2} \sum_i n_i \alpha_i G'(M_i^2) = 0, \quad (6)$$

with $G'(\eta) = \partial G(\eta)/\partial \eta$. The further condition

$$-\frac{\lambda_{\phi H}}{2\lambda_H} = \frac{v^2}{x^2} + \sum_i \frac{n_i \alpha_i}{\lambda_H x^2} G'(M_i^2), \quad (7)$$

is also satisfied. Absent fine-tuning, we observe that with $\lambda_{H,\phi_H} = \mathcal{O}(1)$ one obtains $v \sim x$ and the exotic scale is expected near the TeV scale. Eqs. (6) and (7) ensure that the tadpoles vanish.

One-loop vacuum stability requires that the couplings obey:

$$\lambda_H^{1-l}, \lambda_\phi^{1-l}, \lambda_{\phi_H}^{1-l} + 2\sqrt{\lambda_H^{1-l}\lambda_\phi^{1-l}} > 0, \quad (8)$$

where the one-loop couplings are defined as

$$\lambda_H^{1-l} = \frac{1}{6} \frac{\partial^4 V_{1-l}}{\partial h^4}, \quad \lambda_\phi^{1-l} = \frac{1}{6} \frac{\partial^4 V_{1-l}}{\partial \phi^4}, \quad \lambda_{\phi_H}^{1-l} = \frac{\partial^4 V_{1-l}}{\partial h^2 \partial \phi^2}. \quad (9)$$

Eq. (8) guarantees that the masses for the neutral scalars h and ϕ are strictly positive, forcing one of the beyond-SM scalars in the doublet S to be the heaviest particle in the spectrum, to overcome top-quark contributions to the dilaton mass. Demanding $\lambda_{\phi_H}^{1-l} < 0$ also ensures that the vacuum with $v \neq 0$ and $x \neq 0$ is preferred over the vacuum with a single nonzero VEV.

2.2 The Scalar Spectrum

Writing the inert-doublet as $S = (S^+, (S^0 + iA)/\sqrt{2})^T$, the components have masses

$$\begin{aligned} M_{S^+}^2 &= \frac{\lambda_{\phi S}}{2} x^2 + \frac{\lambda_3}{2} v^2, \\ M_{S^0, A}^2 &= \frac{\lambda_{\phi S}}{2} x^2 + (\lambda_3 + \lambda_4 \pm \lambda_5) \frac{v^2}{2} = M_{S^+}^2 + (\lambda_4 \pm \lambda_5) \frac{v^2}{2}. \end{aligned} \quad (10)$$

The λ_5 -term splits the neutral scalar masses M_{S^0} and M_A , with the splitting becoming negligible in the limit $\lambda_5 \ll 1$.² After symmetry breaking, the scalars h and ϕ mix to give two mass eigenstates, which we denote by $h_{1,2}$,

$$h_1 = h \cos \theta_h - \phi \sin \theta_h, \quad h_2 = h \sin \theta_h + \phi \cos \theta_h. \quad (11)$$

Due to the Z_2 symmetry, the neutral components of S do not mix with these fields. At tree-level the mixing angle is determined by the VEVs,

$$c_h \equiv \cos \theta_h = \frac{x}{\sqrt{x^2 + v^2}}, \quad s_h \equiv \sin \theta_h = \frac{v}{\sqrt{x^2 + v^2}}, \quad (12)$$

and the SM-like scalar mass is given by

$$M_{h_1}^2 = (2\lambda_H - \lambda_{\phi_H})v^2 \simeq 125 \text{ GeV}. \quad (13)$$

²Note that the limit $\lambda_5 \ll 1$ is technically natural due to the restoration of lepton number symmetry in the limit $\lambda_5 \rightarrow 0$.

The scalar h_2 is the pseudo-Goldstone boson associated with the broken SI symmetry, and is massless at tree-level, though radiative corrections induce $M_{h_2} \neq 0$. A useful approximation for M_{h_2} is [13]

$$M_{h_2}^2 \simeq \frac{1}{8\pi^2(x^2 + v^2)} \left\{ M_{h_1}^4 + 6M_W^4 + 3M_Z^4 - 12M_t^4 + 2M_{S^+}^4 + M_A^4 + M_{S^0}^4 - 2 \sum_{i=1}^3 M_i^4 \right\}. \quad (14)$$

Here the singlet fermion masses are given by $M_i = y_i x$, and are ordered as $M_1 < M_2 < M_3$. Eq. (14) shows that viable symmetry breaking requires one of the scalars S^+ , S^0 or A to be the heaviest particle in the spectrum, to overcome negative loop contributions to M_{h_2} from the top quark and the fermions N_i .

Tree-level expressions for M_{h_1} and θ_h are presented above for convenience, however, in our numerical analysis (detailed below), we use the mass eigenvalues $M_{h_{1,2}}$ and the mixing angle θ_h obtained by diagonalizing the one-loop corrected potential. We note that the SI symmetry imposes non-trivial constraints on the model, with λ_ϕ and λ_{ϕ_H} fixed by Eqs. (6) and (7), and the Higgs mass $M_{h_1} \simeq 125$ GeV further fixes λ_H .

3 Neutrino Mass

The combined terms in Eqs. (1) and (2) explicitly break lepton number symmetry, giving rise to radiative neutrino mass at the one-loop level, as shown in Figure 1. Observe that ϕ plays a key role in allowing the neutrino mass diagram, without which neutrinos would remain massless.³ Calculating the mass diagram gives

$$(\mathcal{M}_\nu)_{\alpha\beta} = \sum_i \frac{g_{i\alpha} g_{i\beta} M_i}{16\pi^2} \left\{ \frac{M_{S^0}^2}{M_{S^0}^2 - M_i^2} \ln \frac{M_{S^0}^2}{M_i^2} - \frac{M_A^2}{M_A^2 - M_i^2} \ln \frac{M_A^2}{M_i^2} \right\}. \quad (15)$$

In the limit that $M_{S^0}^2 \approx M_A^2 \equiv M_0^2$, this simplifies to

$$(\mathcal{M}_\nu)_{\alpha\beta} \simeq \sum_i \frac{g_{i\alpha} g_{i\beta} \lambda_5 v^2}{16\pi^2} \frac{M_i}{M_0^2 - M_i^2} \left\{ 1 - \frac{M_i^2}{M_0^2 - M_i^2} \ln \frac{M_0^2}{M_i^2} \right\}. \quad (16)$$

Note that the Z_2 symmetry prevents mixing between SM neutrinos and the exotics N_i .

One can relate the entries in the neutrino mass matrix to the elements of the Pontecorvo-Maki-Nakawaga-Sakata (PMNS) mixing matrix [15] elements. We parameterize the latter as

$$U_\nu = \begin{pmatrix} c_{12}c_{13} & c_{13}s_{12} & s_{13}e^{-i\delta_d} \\ -c_{23}s_{12} - c_{12}s_{13}s_{23}e^{i\delta_d} & c_{12}c_{23} - s_{12}s_{13}s_{23}e^{i\delta_d} & c_{13}s_{23} \\ s_{12}s_{23} - c_{12}c_{23}s_{13}e^{i\delta_d} & -c_{12}s_{23} - c_{23}s_{12}s_{13}e^{i\delta_d} & c_{13}c_{23} \end{pmatrix} \times U_m, \quad (17)$$

³The Feynman diagram in Figure 1 is an example of the SI type T3 one-loop topology. Related variants are possible [14].

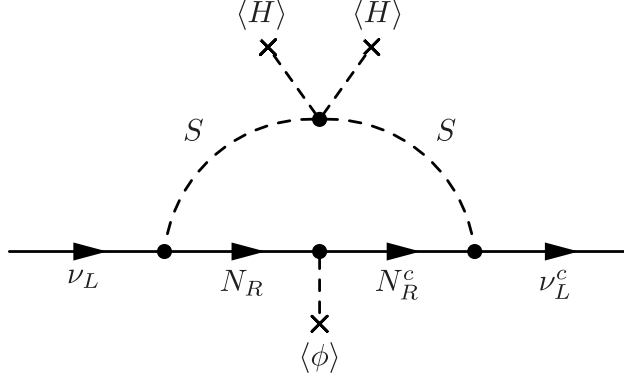


Figure 1: One-loop diagram for neutrino mass in the scale-invariant scotogenic model.

with δ_d being the Dirac phase and $U_m = \text{diag}(1, e^{i\theta_\alpha/2}, e^{i\theta_\beta/2})$ giving the dependence on the Majorana phases $\theta_{\alpha,\beta}$. We use the shorthand $s_{ij} \equiv \sin \theta_{ij}$ and $c_{ij} \equiv \cos \theta_{ij}$ to refer to the mixing angles. In our numerical scans of the parameter space in the model, we fit to the best-fit experimental values for the mixing angles: $s_{13}^2 = 0.025_{-0.003}^{+0.003}$, $s_{12}^2 = 0.320_{-0.017}^{+0.016}$, $s_{23}^2 = 0.43_{-0.03}^{+0.03}$, and the mass-squared differences: $\Delta m_{21}^2 = 7.62_{-0.19}^{+0.19} \times 10^{-5} \text{eV}^2$ and $|\Delta m_{13}^2| = 2.55_{-0.09}^{+0.06} \times 10^{-3} \text{eV}^2$ [16].

To determine the parameter space that generates viable neutrino masses, we use the Casas-Ibarra parameterization [17]

$$(\mathcal{M}_\nu)_{\alpha\beta} = \sum_i g_{i\alpha} g_{i\beta} \Lambda_i = (g^T \Lambda g)_{\alpha\beta}, \quad (18)$$

with

$$\Lambda_i = \frac{M_i}{16\pi^2} \left\{ \frac{M_{S_0}^2}{M_{S_0}^2 - M_i^2} \ln \frac{M_{S_0}^2}{M_i^2} - \frac{M_A^2}{M_A^2 - M_i^2} \ln \frac{M_A^2}{M_i^2} \right\}. \quad (19)$$

According to the Casas-Ibarra parameterization, the coupling g can be written as

$$g = D_{\sqrt{\Lambda^{-1}}} \mathcal{R} D_{\sqrt{m_\nu}} U_\nu^\dagger, \quad (20)$$

where $D_{\sqrt{\Lambda^{-1}}} = \text{diag} \left\{ \sqrt{\Lambda_1^{-1}}, \sqrt{\Lambda_2^{-1}}, \sqrt{\Lambda_3^{-1}} \right\}$, $D_{\sqrt{m_\nu}} = \text{diag} \left\{ \sqrt{m_1}, \sqrt{m_2}, \sqrt{m_3} \right\}$, and \mathcal{R} is an orthogonal rotation matrix ($m_{1,2,3}$ are the neutrino eigen-masses).

4 Invisible Higgs Decays

The model is subject to constraints on the branching fraction for invisible Higgs decays, $\mathcal{B}(h \rightarrow inv) < 17\%$ [18]. One should use $inv \equiv \{h_2 h_2\}, \{N_{\text{DM}} N_{\text{DM}}\}$, when kinematically

available, with corresponding decay widths given by

$$\begin{aligned}\Gamma(h_1 \rightarrow h_2 h_2) &= \frac{1}{32\pi} \frac{(\lambda_{122})^2}{M_{h_1}} \left(1 - \frac{4M_{h_2}^2}{M_{h_1}^2}\right)^{\frac{1}{2}} \Theta(M_{h_1} - 2M_{h_2}), \\ \Gamma(h_1 \rightarrow N_{\text{DM}} N_{\text{DM}}) &= \frac{\tilde{y}_{\text{DM}}^2 s_h^2}{16\pi} M_{h_1} \left(1 - \frac{4M_{\text{DM}}^2}{M_{h_1}^2}\right)^{\frac{3}{2}} \Theta(M_{h_1} - 2M_{\text{DM}}).\end{aligned}\quad (21)$$

The effective cubic coupling λ_{122} is defined in Eq. (35) below. As a result of the SI symmetry, the coupling λ_{122} vanishes at tree-level, and the non-zero loop-level coupling is sufficiently small to ensure that decay to h_2 pairs is highly suppressed.⁴

5 Lepton Flavor Violating Decays

The new fields give rise to one-loop contributions to $\mu \rightarrow e + \gamma$. Normalized relative to $\text{Br}(\mu \rightarrow e\nu_\mu\bar{\nu}_e)$, the corresponding branching fraction is

$$\frac{\text{Br}(\mu \rightarrow e\gamma)}{\text{Br}(\mu \rightarrow e\nu_\mu\bar{\nu}_e)} = \frac{3(4\pi)^3 \alpha_{em}}{4G_F^2} |A_D|^2, \quad (22)$$

where A_D is the dipole form factor:

$$A_D = \sum_i \frac{g_{ei}^* g_{i\mu}}{32\pi^2} \frac{1}{M_{S^+}^2} F^{(n)}(M_i^2/M_{S^+}^2). \quad (23)$$

with the loop function given by

$$F^{(n)}(x) = [1 - 6x + 3x^2 + 2x^3 - 6x^2 \ln x]/[6(1-x)^4]. \quad (24)$$

A simple change of labels allows one to use the above formulae for the related decay $\tau \rightarrow \mu + \gamma$. In our analysis we also include the constraint from neutrino-less double beta decay.

Note that, in general, the scotogenic model is subject to strong LFV constraints, relating to the fact that the DM annihilates via the same Yukawa couplings that mediate LFV processes. Consequently one cannot decouple the two effects and there can be tension between the demands of suppressed LFV processes and the attainment of a viable DM abundance (actually, in the scotogenic model, constraints from other LFV processes, like μ - e conversion, can be more severe than the above LFV decays; see the 3rd and 4th papers in Ref. [2]). However, we shall see that the situation differs in the SI model, due to additional annihilation processes mediated by the dilaton. This provides a degree of decoupling between the LFV processes and DM annihilations, such that LFV bounds are more readily satisfied. Thus, for our purposes, it is sufficient to consider the above LFV decays (we shall see that

⁴Note that h_2 decays to SM states, similar to a light SM Higgs boson but with suppression by the mixing angle, s_h^2 . However, dedicated ATLAS or CMS searches for such light scalars, in the channels $2b$, 2τ or 2γ , do not currently exist, so we classify the decay $h_1 \rightarrow h_2 h_2$ as invisible. In practice, however, the suppression of $\Gamma(h_1 \rightarrow h_2 h_2)$ due to SI symmetry renders this point moot.

the viable parameter space includes regions well-below the LFV bounds, so slightly stronger bounds do not have a large effect). We note that the correlation between $\mu \rightarrow e\gamma$ and the DM relic abundance, for the case of fermionic DM in the scotogenic model, was first noted in Ref. [19], while Ref. [20] noted that models with a singlet scalar allow one to decouple these issues.

6 Dark Matter

6.1 Relic Density

As the universe cools, the temperature eventually drops below the DM mass. Consequently the DM number density becomes Boltzmann suppressed and the DM annihilation rate can become comparable to the Hubble parameter. At a certain temperature the DM particles freeze out of equilibrium, such that the DM number density in a comoving volume henceforth remains constant. The cold DM relic abundance therefore depends on the total thermally averaged annihilation cross section

$$\begin{aligned} \langle \sigma(N_{\text{DM}} N_{\text{DM}})v_r \rangle &= \sum_X \langle \sigma(N_{\text{DM}} N_{\text{DM}} \rightarrow X)v_r \rangle \\ &= \sum_X \int_{4M_{\text{DM}}^2}^{\infty} ds \sigma_{N_{\text{DM}} N_{\text{DM}} \rightarrow X}(s) \frac{(s - 4M_{\text{DM}}^2)}{8TM_{\text{DM}}^4 K_2^2 \left(\frac{M_{\text{DM}}}{T}\right)} \sqrt{s} K_1 \left(\frac{\sqrt{s}}{T}\right), \end{aligned} \quad (25)$$

where v_r is the relative velocity, s is the Mandelstam variable, $K_{1,2}$ are the modified Bessel functions and $\sigma_{N_{\text{DM}} N_{\text{DM}} \rightarrow X}(s)$ is the annihilation cross due to the channel $N_{\text{DM}} N_{\text{DM}} \rightarrow X$, at the CM energy \sqrt{s} . At freeze-out, the thermal relic density can be given in terms of the thermally averaged annihilation cross section by

$$\Omega_{\text{DM}} h^2 \simeq \frac{(1.07 \times 10^9) x_F}{\sqrt{g_*} M_{pl}(\text{GeV}) \langle \sigma(N_{\text{DM}} N_{\text{DM}})v_r \rangle}, \quad (26)$$

where M_{pl} is the Plank mass and g_* counts the effective degrees of freedom of the relativistic fields in equilibrium. The inverse freeze-out temperature, $x_F = M_{\text{DM}}/T_F$, can be determined iteratively from the equation

$$x_F = \log \left(\sqrt{\frac{45}{8}} \frac{M_{\text{DM}} M_{pl} \langle \sigma(N_{\text{DM}} N_{\text{DM}})v_r \rangle}{\pi^3 \sqrt{g_*} x_F} \right). \quad (27)$$

In the present model, the classes of DM annihilation channels are shown in Fig. 2. The DM can annihilate into: (1) charged leptons and neutrinos, $\ell_\alpha^- \ell_\beta^+$ and $\nu_\alpha \bar{\nu}_\beta$, including LFV final states with $\alpha \neq \beta$, (2) SM fermions and gauge bosons $b\bar{b}$, $t\bar{t}$, W^+W^- , ZZ and the scalars SS , and (3) final states comprised of the Higgs and/or dilaton, $h_i h_k$. The first class of channels are $h_{1,2}$ -mediated s -channel processes, the second class are S -mediated t -channel processes while the third class contains both s - and t -channels processes mediated by $h_{1,2}$.

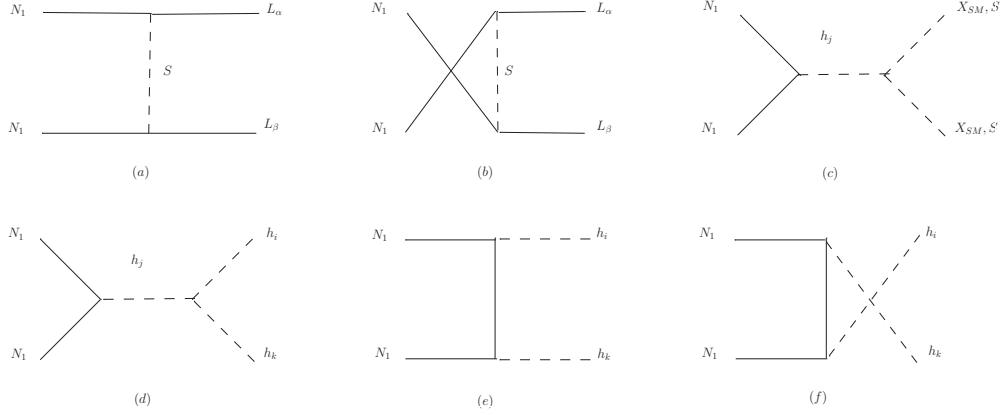


Figure 2: Diagrams for DM annihilation.

6.2 Annihilation Cross Sections

(1) t-channel processes

The cross section for the annihilation channel into charged leptons⁵ is given by [21]

$$\sigma(N_{\text{DM}}N_{\text{DM}} \rightarrow \ell_{\alpha}^{-}\ell_{\beta}^{+})v_r = \frac{1}{8\pi s} \frac{|g_{1\alpha}g_{1\beta}^*|^2}{(M_{S^+}^2 - M_{\text{DM}}^2 + \frac{s}{2})^2} \left[\frac{m_{\ell_{\alpha}}^2 + m_{\ell_{\beta}}^2}{2} \left(\frac{s}{2} - M_{\text{DM}}^2 \right) \right. \\ \left. + \frac{2}{3}s \left(\frac{s}{4} - M_{\text{DM}}^2 \right) \frac{(M_{S^+}^2 - M_{\text{DM}}^2)^2 + \frac{s}{2}(M_{S^+}^2 - M_{\text{DM}}^2) + \frac{s^2}{8}}{(M_{S^+}^2 - M_{\text{DM}}^2 + \frac{s}{2})^2} \right]. \quad (28)$$

The cross section for annihilation into neutrinos can be obtained from Eq. (28) by replacing $M_{S^+}^2 \rightarrow M_{S^0}^2$ and sending the charged lepton masses to zero, i.e.,

$$\sigma(N_{\text{DM}}N_{\text{DM}} \rightarrow \nu_{\alpha}\nu_{\beta})v_r = \frac{|g_{1\alpha}g_{1\beta}^*|^2}{12\pi} \left(\frac{s}{4} - M_{\text{DM}}^2 \right) \frac{(M_{S^0}^2 - M_{\text{DM}}^2)^2 + \frac{s}{2}(M_{S^0}^2 - M_{\text{DM}}^2) + \frac{s^2}{8}}{(M_{S^0}^2 - M_{\text{DM}}^2 + \frac{s}{2})^4}. \quad (29)$$

(2) s-channel processes

The processes $N_{\text{DM}}N_{\text{DM}} \rightarrow b\bar{b}, t\bar{t}, W^+W^-$ and ZZ can occur as shown in Fig. 2-c. The corresponding amplitude can be written as

$$\mathcal{M} = ic_h s_h y_1 \bar{u}(k_2) u(k_1) \left(\frac{i}{s - M_{h_1}^2} - \frac{i}{s - M_{h_2}^2} \right) \mathcal{M}_{h \rightarrow SM} (m_h \rightarrow \sqrt{s}), \quad (30)$$

with $\mathcal{M}_{h \rightarrow SM} (m_h \rightarrow \sqrt{s})$ being the amplitude of the Higgs decay $h \rightarrow X_{SM}\bar{X}_{SM}$, with the Higgs mass replaced as $m_h \rightarrow \sqrt{s}$. This leads to the cross section

$$\sigma(N_{\text{DM}}N_{\text{DM}} \rightarrow X_{SM}\bar{X}_{SM})v_r = 8\sqrt{s} s_h^2 c_h^2 y_1^2 \left| \frac{1}{s - M_{h_1}^2} - \frac{1}{s - M_{h_2}^2} \right|^2 \Gamma_{h \rightarrow X_{SM}\bar{X}_{SM}} (m_h \rightarrow \sqrt{s}), \quad (31)$$

⁵For same-flavor charged leptons ($\alpha = \beta$), there are also s -channel processes mediated by $h_{1,2}$. However, these are proportional to their Yukawa couplings and may therefore be ignored.

where $\Gamma_{h \rightarrow X_{SM} \bar{X}_{SM}} (m_h \rightarrow \sqrt{s})$ is the total decay width, with $m_h \rightarrow \sqrt{s}$.

Similarly, the SS annihilation cross section can be written as

$$\sigma(N_{\text{DM}} N_{\text{DM}} \rightarrow SS) v_r = \eta_S \frac{s_h^2 c_h^2 y_1^2}{4\pi} s \left| \frac{c_h \lambda_{1SS}}{s - M_{h_1}^2 - iM_{h_1} \Gamma_{h_1}} + \frac{s_h \lambda_{2SS}}{s - M_{h_2}^2 - iM_{h_2} \Gamma_{h_2}} \right|^2 \left(1 - \frac{4M_S^2}{s} \right)^{1/2} \quad (32)$$

where $\eta_{S^0} = \eta_A = 1$, $\eta_{S^+} = 2$, and λ_{1SS} and λ_{2SS} are the triple couplings of a scalar $h_{1,2}$ with two S fields, given by

$$\begin{aligned} \lambda_{1S^+S^-} &= \lambda_3 c_h v - \lambda_{\phi S} s_h x, & \lambda_{2S^+S^-} &= \lambda_3 s_h v + \lambda_{\phi S} c_h x, \\ \lambda_{1S^0S^0,1AA} &= \frac{1}{2} (\lambda_3 + \lambda_4 \pm \lambda_5) c_h v - \frac{1}{2} \lambda_{\phi S} s_h x, \\ \lambda_{2S^0S^0,2AA} &= \frac{1}{2} (\lambda_3 + \lambda_4 \pm \lambda_5) s_h v + \frac{1}{2} \lambda_{\phi S} c_h x. \end{aligned} \quad (33)$$

(3) Higgs channel

The DM can self-annihilate into $h_i h_k$, as seen in Fig. 2-d, -e and -f. The amplitude squared is given by

$$\begin{aligned} |\mathcal{M}|^2 &= 2\tilde{y}_{\text{DM}}^2 s \left[\frac{c_h \lambda_{1ik}}{s - M_{h_1}^2} + \frac{s_h \lambda_{2ik}}{s - M_{h_2}^2} \right]^2 \\ &+ 4c_i c_k \tilde{y}_{\text{DM}}^3 M_{\text{DM}} \left[\frac{c_h \lambda_{1ik}}{s - M_{h_1}^2} + \frac{s_h \lambda_{2ik}}{s - M_{h_2}^2} \right] \left(\frac{s - M_{h_i}^2 + M_{h_k}^2}{t - M_{\text{DM}}^2} + a \frac{s + M_{h_i}^2 - M_{h_k}^2}{u - M_{\text{DM}}^2} \right) \\ &+ \frac{2c_i^2 c_k^2 \tilde{y}_{\text{DM}}^4}{(t - M_{\text{DM}}^2)^2} \left\{ 4M_{\text{DM}}^2 M_{h_k}^2 + (M_{\text{DM}}^2 + M_{h_i}^2 - t) (M_{\text{DM}}^2 + M_{h_i}^2 - u) - s M_{h_i}^2 \right\} \\ &+ a^2 \frac{2c_i^2 c_k^2 \tilde{y}_{\text{DM}}^4}{(u - M_{\text{DM}}^2)^2} \left\{ 4M_{\text{DM}}^2 M_{h_i}^2 + (M_{\text{DM}}^2 + M_{h_k}^2 - u) (M_{\text{DM}}^2 + M_{h_k}^2 - t) - s M_{h_k}^2 \right\} \\ &+ a \frac{2c_i^2 c_k^2 \tilde{y}_{\text{DM}}^4}{(t - M_{\text{DM}}^2) (u - M_{\text{DM}}^2)} \left\{ (M_{\text{DM}}^2 + M_{h_i}^2 - t) (M_{\text{DM}}^2 + M_{h_k}^2 - t) \right. \\ &\left. + (M_{\text{DM}}^2 + M_{h_k}^2 - u) (M_{\text{DM}}^2 + M_{h_i}^2 - u) - (s - 4M_{\text{DM}}^2) (s - M_{h_i}^2 - M_{h_k}^2) \right\}, \end{aligned} \quad (34)$$

with s , t and u being the Mandelstam variables, and the Yukawa couplings are defined as $\tilde{y}_{\text{DM}} \equiv y_1$, $c_1 \equiv c_h$ and $c_2 \equiv s_h$. Here, we integrate the phase space numerically to obtain the cross section for a given value of s . At tree-level the effective cubic scalar couplings (λ_{1ik} and λ_{2ik}) are given by

$$\begin{aligned} \lambda_{111} &= 6\lambda_{\text{H}} c_h^3 v - 3\lambda_{\phi\text{H}} c_h^2 s_h v + 3\lambda_{\phi\text{H}} c_h s_h^2 x - 6\lambda_{\phi} s_h^3 x, \\ \lambda_{112} &= \lambda_{\phi\text{H}} c_h^3 x + 2c_h^2 s_h (3\lambda_{\text{H}} - \lambda_{\phi\text{H}}) v + 2c_h s_h^2 (3\lambda_{\phi} - \lambda_{\phi\text{H}}) x + \lambda_{\phi\text{H}} s_h^3 v, \\ \lambda_{222} &= \lambda_{122} = 0, \end{aligned} \quad (35)$$

though for completeness we employ the one-loop results, obtained from the loop-corrected potential following Ref. [22]. We note that the (leading order) absence of the cubic interactions $h_1 h_2^2$ and h_2^3 , is a general feature of SI models.

6.3 Direct Detection

With regard to direct-detection experiments, interactions between the DM and quarks are described by an effective low-energy Lagrangian:

$$\mathcal{L}_{N_1-q}^{(eff)} = a_q \bar{q}q N_{\text{DM}}^c N_{\text{DM}}, \quad (36)$$

with

$$a_q = -\frac{s_h c_h M_q M_{\text{DM}}}{2 \langle \phi \rangle \langle H^0 \rangle} \left[\frac{1}{M_{h_1}^2} - \frac{1}{M_{h_2}^2} \right]. \quad (37)$$

Consequently, the effective nucleon-DM interaction is written as

$$\mathcal{L}_{\text{DM}-\mathcal{N}}^{(eff)} = a_{\mathcal{N}} \bar{\mathcal{N}}\mathcal{N} N_{\text{DM}}^c N_{\text{DM}},$$

where

$$a_{\mathcal{N}} = \frac{s_h c_h (M_{\mathcal{N}} - \frac{7}{9} M_{\mathcal{B}}) M_{\text{DM}}}{\langle \phi \rangle \langle H^0 \rangle} \left[\frac{1}{M_{h_1}^2} - \frac{1}{M_{h_2}^2} \right]. \quad (38)$$

In this relation, $M_{\mathcal{N}}$ is the nucleon mass and $M_{\mathcal{B}}$ the baryon mass in the chiral limit [23]. This leads to the following nucleon-DM elastic cross section in the chiral limit

$$\sigma_{\text{det}} = \frac{s_h^4 M_{\mathcal{N}}^2 (M_{\mathcal{N}} - \frac{7}{9} M_{\mathcal{B}})^2 M_{\text{DM}}^4}{\pi \langle H^0 \rangle^4 (M_{\text{DM}} + M_{\mathcal{B}})^2} \left[\frac{1}{M_{h_1}^2} - \frac{1}{M_{h_2}^2} \right]^2. \quad (39)$$

The analysis below will show that the upper bound reported by LUX experiment [26] provides a stringent constraint on σ_{det} .

7 Analysis and Results

Next we turn to our numerical analysis and results. We perform a numerical scan of the parameter space to determine whether radiative electroweak symmetry breaking is compatible with one-loop radiative neutrino mass and singlet neutrino DM. In the scans, we enforce the minimization conditions, Eqs. (6) and (7), vacuum stability via Eq. (8), and demand that the SM-like Higgs mass is in the experimentally allowed range, $M_{h_1} = 125.09 \mp 0.21$ GeV. Compatibility with constraints from LEP (OPAL) on a light Higgs [24] are enforced, and we consider the constraint from the Higgs invisible decay, $\mathcal{B}(h \rightarrow inv) < 17\%$, [18]. Dimensionless couplings are restricted to the perturbative range throughout, and we consider values of $100 \text{ GeV} < \langle \phi \rangle < 5 \text{ TeV}$ for the beyond-SM VEV (however, we only find viable benchmark points for $\langle \phi \rangle \gtrsim 150 \text{ GeV}$).⁶

The scan reveals a spread of viable values for the dilaton mass M_{h_2} , consistent with OPAL, as plotted in Figure 3. In the scan we tend to find M_{h_2} in the range $\mathcal{O}(1) \text{ GeV} \lesssim M_{h_2} \lesssim 90 \text{ GeV}$. Lighter values of M_{h_2} seemingly require an amount of engineered cancellation

⁶In principle, one can consider larger values for $\langle \phi \rangle$. However, these require hierarchically small couplings in the scalar potential [25], which we do not consider here.

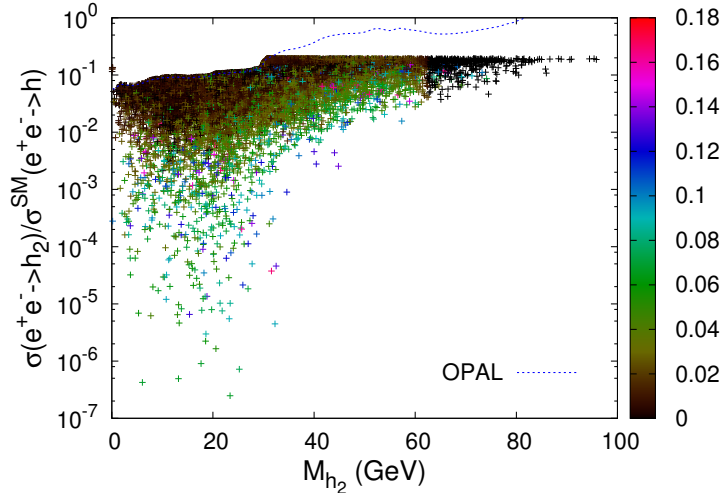


Figure 3: Scalar mixing versus the light scalar mass M_{h_2} . The palette shows the branching ratio for invisible Higgs decays. An overwhelming majority of the points satisfy the constraint $B(h_1 \rightarrow inv) < 17\%$.

among the radiative mass-corrections from fermions and bosons, or larger values for $\langle\phi\rangle$; see Eq. (14). We noticed that regions with $\langle\phi\rangle \gtrsim 500$ GeV tend to be preferred.

We further scan for parameter space giving viable neutrino masses and mixing, subject to the LFV and muon anomalous magnetic moment constraints, while simultaneously generating a viable DM relic density. Figure 4 shows viable benchmark sets for the Yukawa couplings $g_{i\alpha}$, along with the corresponding LFV branching ratios and δa_μ contributions. The couplings $g_{i\alpha}$ are typically well-below the perturbative bound. Note that the range for the Yukawa couplings varies over several orders of magnitude. This reflects the freedom to take the lepton-number violating quartic coupling λ_5 to be small, and accordingly transfer some of the neutrino mass suppression between the Yukawa and quartic coupling sectors. The capacity to obtain viable neutrino masses, with Yukawa couplings that vary over a considerable range, influences the strength of the signal from LFV decays. Figure 4 shows that the bound from $\mu \rightarrow e\gamma$ gives important constraints in parameter space with larger $g_{i\alpha}$, while smaller values of $g_{i\alpha}$ allow the model to easily evade the bound. Constraints from the weaker $\tau \rightarrow \mu\gamma$ bound are readily satisfied. Also, we verified that constraints from neutrino-less double-beta decay searches are satisfied by the benchmark points.

With regards to the DM relic density, recall that there are multiple classes of annihilation channels, namely $N_{\text{DM}}N_{\text{DM}} \rightarrow X$ ($X = \ell_\alpha^\mp \ell_\beta^\pm, \nu_\alpha \nu_\beta, b\bar{b}, t\bar{t}, WW, ZZ, SS, h_{1,2}h_{1,2}$). Depending on the specific value of the DM mass, a given channel may be significant or suppressed. To probe the role of the distinct channels, in Figure 5-left we plot the contribution of each channel relative to the total cross section at freeze-out, $\sigma_X/\sigma_{\text{tot}}$, versus the DM mass. Annihilations into lepton pairs typically play a subdominant role. These are mediated by the couplings $g_{i\alpha}$, whose values should be sufficiently small to ensure viable neutrino masses and consistency with LFV constraints. For lighter values of $M_{\text{DM}} \lesssim 75$ GeV, the cross section

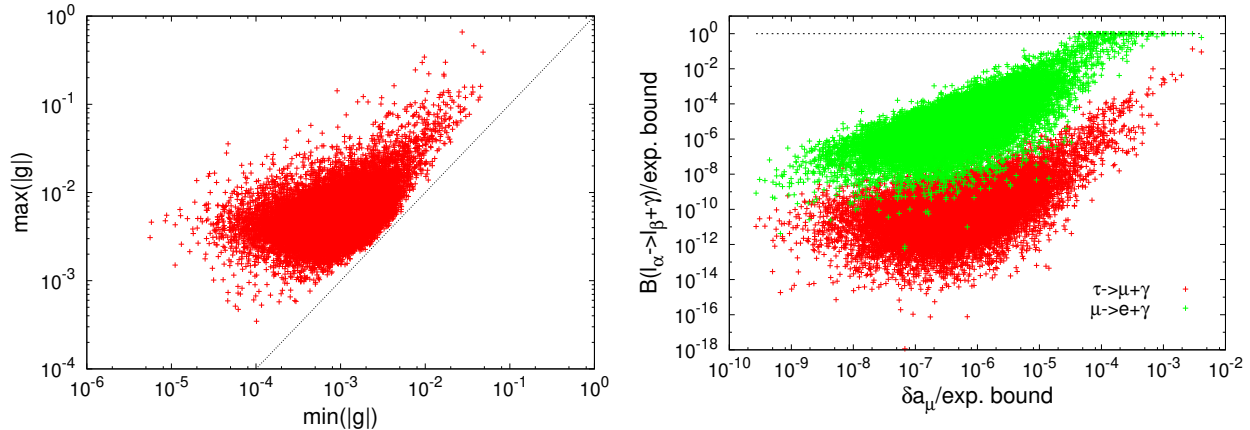


Figure 4: Left: Viable benchmark points for the Yukawa couplings $g_{i\alpha}$, in absolute values. The dashed line denotes the degenerate case, i.e, $\min |g| = \max |g|$. Right: The LFV branching ratios versus the muon anomalous magnetic moment, both scaled by the experimental bounds.

tends to be dominated by annihilations into b quarks, while annihilations into Z_2 -even neutral scalar final states ($X = hh$ with $h \equiv h_{1,2}$) are dominant for heavier values of $M_{\text{DM}} \gtrsim 125$ GeV. In the intermediate range, annihilations into gauge bosons can also be important. For completeness, we include the final states $X = 2S$ in the plot, for components of the doublet S . Although the doublet scalars are typically heavier than the DM, thermal fluctuations can allow a contribution from these modes (though the effect is clearly subdominant, as seen in the Figure). Figure 5-right shows the mass of the charged scalar, M_{S^+} , versus the DM mass. In the lighter DM mass range, $M_{\text{DM}} \lesssim \mathcal{O}(100)$ GeV, one notices that the charged scalar mass should not exceed 450 GeV, while for larger values of M_{DM} one can have M_{S^+} at the TeV scale. Such light charged scalars may be of phenomenological interest as they can be within reach of collider experiments.

We note that Figure 5-right contains disconnected regions for viable DM, with the region $31 \text{ GeV} \lesssim M_{\text{DM}} \lesssim 48 \text{ GeV}$ not returning viable benchmark points. This “missing region” results from an over-abundance of DM, due to an insufficiently large, thermally-averaged annihilation cross section. In the small M_{DM} region, the annihilation cross section is dominated by $b\bar{b}$ final states, with an important sub-contribution from annihilations into dilatons. However, below $M_{\text{DM}} \approx 48$ GeV, we find that the dilaton contribution is too small to allow the observed relic abundance. The allowed island at $M_{\text{DM}} \lesssim 31$ GeV corresponds to parameter space that approaches the h_2 resonance, such that $2M_{\text{DM}}$ is around, or just below, the dilaton mass, namely $M_{\text{DM}} \lesssim M_{h_2}/2$ (the dilaton mass is shown in Figure 6). This enhances annihilations into SM final states. The corresponding enhancement to the s -channel process $N_{\text{DM}}N_{\text{DM}} \rightarrow h_2h_2$, via an intermediate h_2 , is not sufficient to overcome the small cubic coupling λ_{222} , as shown in Eq. (35). Note also that points in the region $M_{\text{DM}} \lesssim M_{h_1}/2 \approx 60$ GeV experience some enhancement from the h_1 resonance. Such enhancements do not occur in heavier M_{DM} regions, as both the dilaton and Higgs are much lighter than the DM. Throughout the lighter M_{DM} regions, the Higgs may decay into N_{DM}

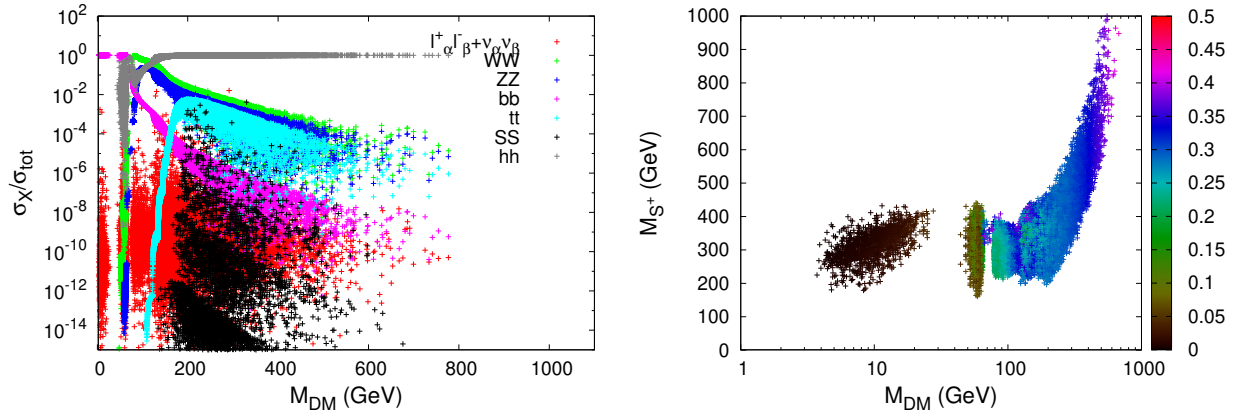


Figure 5: Left: The cross section ratio $\sigma_X/\sigma_{\text{tot}}$ at freeze-out versus the DM mass. Here X denotes lepton pairs, gauge bosons, heavy quarks and scalars. Right: The charged scalar masses M_{S^+} versus the DM mass. The palette shows the DM Yukawa coupling $y_{\text{DM}} \equiv y_1$.

and h_2 final states, though the bound on invisible Higgs decays is readily satisfied. The decay $h_1 \rightarrow N_{\text{DM}}N_{\text{DM}}$ is sufficiently small due to Yukawa suppression (in addition to small θ_h mixing), as seen from the palette in Figure 5-right, while the decay $h_1 \rightarrow h_2h_2$ is suppressed by the small cubic scalar coupling λ_{122} .

Next we consider the constraints from direct-detection experiments. We plot the direct-detection cross section versus the DM mass for the benchmark parameter sets in Figure 6. The mass of the dilaton, M_{h_2} , in units of GeV, is shown in the corresponding palette. One immediately observes that direct-detection limits from LUX [26] impose very serious constraints on the model, with a large number of benchmark sets already excluded. The plot shows that the surviving benchmark points mostly occur for $M_{\text{DM}} \lesssim 10$ GeV, with a smaller number of viable points found for $M_{\text{DM}} \gtrsim 200$ GeV. Benchmarks with intermediate M_{DM} values are excluded. The viable parameter space typically requires a lighter dilaton mass, $M_{h_2} \lesssim 10$ GeV, as all benchmarks with $M_{h_2} \gtrsim 50$ GeV are excluded. It is clear from the figure that the surviving benchmark sets can be probed in forthcoming direct-detection experiments.

In Figure 7 we consider the oblique parameters. The variation with respect to the mixing parameter $\sin^2 \theta_h$ is shown in the left panel. One notices that the $\sin^2 \theta_h$ dependence is not the dominant source of variation. There is some sensitivity to $\sin^2 \theta_h$, primarily in ΔS . However, for a given fixed value of $\sin^2 \theta_h$, benchmark points occur along the majority of the V-shaped curve traced out in the plot. Thus, the $\sin^2 \theta_h$ dependence is not driving the variation. The dependence of the oblique parameters on the dimensionless mass-difference for components of S , namely $\Delta = (2M_{S^+} - M_A - M_{S^0})/2M_{S^+}$, is shown in the right panel of Figure 7. The plot shows that the majority of the variation in ΔT is due to the mass-splitting encoded in Δ . This is expected. The T parameter is sensitive to isospin violation and thus constrains the splitting for $SU(2)_L$ multiplets. Viable benchmark points occur in the region with $\Delta \approx 0$, as seen in the plot, while larger mass-splittings can conflict with the

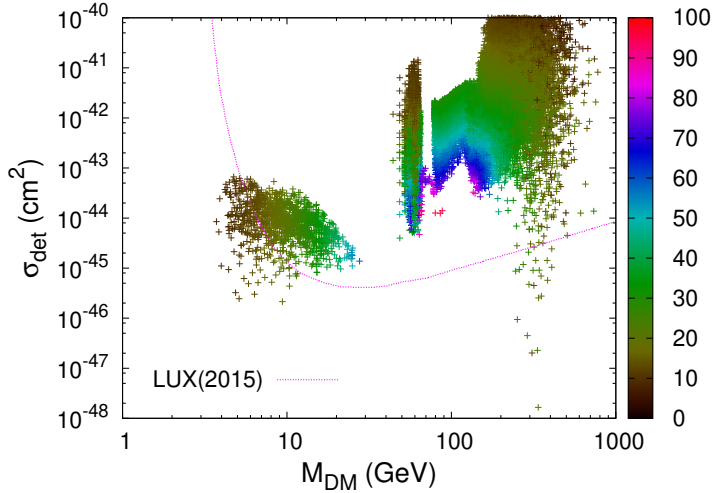


Figure 6: The direct detection cross section versus the DM mass. The dashed line shows the recent constraints from LUX, while the palette gives the mass for the neutral beyond-SM scalar (dilaton), M_{h_2} , in units of GeV.

constraints.

The benchmark points include a range of values for the mass-splitting parameter Δ , giving rise to the variation in Figure 7. However, in general, one can take the couplings $\lambda_{4,5}$ in the scalar potential sufficiently small to ensure the mass-splitting for S^+ , S^0 and A is consistent with oblique constraints. From the (technical) naturalness perspective, arbitrarily small values of λ_5 are allowed, due to the enhanced lepton number symmetry for $\lambda_5 \rightarrow 0$.⁷ Natural values of λ_4 are bounded from below by one-loop gauge contributions to the operator $|H^\dagger S|^2$. Consequently the mass splitting for components of S is not expected to be smaller than the one-loop induced splitting, which is safely within the bounds. Thus, although the oblique parameters can exclude some regions of parameter space, the constraints are readily evaded.

The exotics in the model can also give new contributions to the Higgs decays $h \rightarrow \gamma Z$ and $h \rightarrow \gamma\gamma$. The ratio of the corresponding widths, relative to the SM values, is plotted in Figure 8. One sees that the overwhelming majority of the benchmark points are consistent with constraints from ATLAS and CMS. Importantly, more-precise measurements by ATLAS and CMS during Run II of the LHC will provide further probes of the model.

Before concluding, we note that our analysis reveals considerable differences between the SI scotogenic model and the standard (non-SI) scotogenic model. These relate primarily to the presence of the dilaton. The coupling between ϕ and the DM provides new annihilation channels for the sterile neutrino DM. This alleviates the need for larger Yukawa couplings $g_{i\alpha}$, normally required in the scotogenic model to generate the relic density, and reduces

⁷In practice, the demand of viable neutrino masses gives a Yukawa coupling-dependent lower bound on λ_5 .

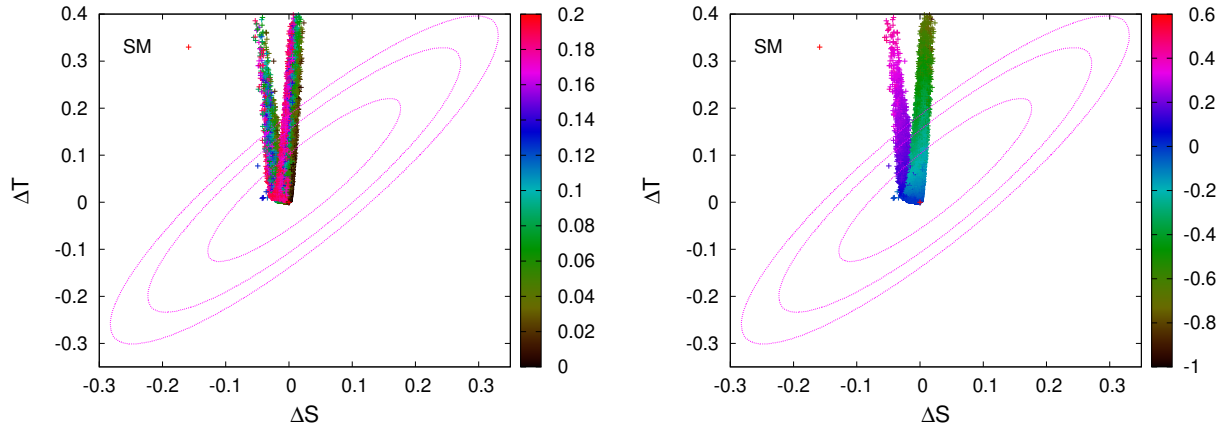


Figure 7: Left: The oblique parameters ΔS versus ΔT for the benchmarks used previously. The ellipsoids show the 68%, 95% and 99% CL., respectively. In the Left frame, the palette shows the mixing $\sin^2 \theta_h$ between the Higgs and the dilaton; in the Right frame it shows the relative mass splitting, $\Delta = (2M_{S^+} - M_A - M_{S^0}) / 2M_{S^+}$, for components of the scalar doublet S .

the tension with LFV constraints. However, the dilaton also permits new channels at direct-detection experiments making these constraints more severe for the SI model. As a rough guide, one expects stronger LFV signals for the scotogenic model, and stronger direct-detection signals for the SI scotogenic model.

8 Conclusion

In this work, we performed a detailed study of the minimal SI scotogenic model. Our analysis demonstrates the existence of viable parameter space in which one obtains radiative electroweak symmetry breaking, one-loop neutrino masses and a good DM candidate. The model predicts a new scalar with $\mathcal{O}(\text{GeV})$ mass. This field plays the dual roles of triggering electroweak symmetry breaking and sourcing lepton number symmetry violation. The model can give observable signals in LFV searches, direct-detection experiments, and precision searches for the Higgs decays $h \rightarrow \gamma\gamma$ and $h \rightarrow \gamma Z$. It also predicts a scalar doublet S , whose mass is expected to be $\lesssim \text{TeV}$, within reach of collider experiments. The model is subject to strong constraints from direct-detection experiments; viable parameter space was found for $M_{\text{DM}} \lesssim 10 \text{ GeV}$ and $M_{\text{DM}} \gtrsim 200 \text{ GeV}$, while intermediate values for M_{DM} appear excluded.

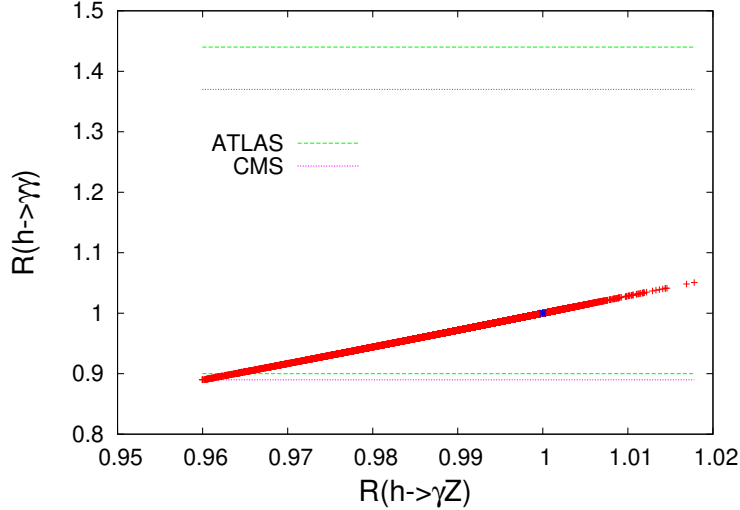


Figure 8: Ratio of the widths for $h \rightarrow \gamma\gamma$ and $h \rightarrow \gamma Z$ relative to the SM values. The constraints from ATLAS and CMS are shown.

Acknowledgments

AA is supported by the Algerian Ministry of Higher Education and Scientific Research under the CNEPRU Project No D01720130042. KM is supported by the Australian Research Council.

References

- [1] E. Ma, Phys. Rev. D **73**, 077301 (2006) [hep-ph/0601225].
- [2] D. Schmidt, T. Schwetz and T. Toma, Phys. Rev. D **85**, 073009 (2012) [arXiv:1201.0906 [hep-ph]]; S. Y. Ho and J. Tandean, Phys. Rev. D **87**, 095015 (2013) [arXiv:1303.5700 [hep-ph]]; T. Toma and A. Vicente, JHEP **1401**, 160 (2014) [arXiv:1312.2840, arXiv:1312.2840 [hep-ph]]; A. Vicente and C. E. Yaguna, JHEP **1502**, 144 (2015) [arXiv:1412.2545 [hep-ph]]; A. Merle and M. Platscher, JHEP **1511**, 148 (2015) [arXiv:1507.06314 [hep-ph]]; M. Hirsch, R. A. Lineros, S. Morisi, J. Palacio, N. Rojas and J. W. F. Valle, JHEP **1310**, 149 (2013) [arXiv:1307.8134 [hep-ph]]. A. Merle, M. Platscher, N. Rojas, J. W. F. Valle and A. Vicente, arXiv:1603.05685 [hep-ph].
- [3] S. R. Coleman and E. J. Weinberg, Phys. Rev. D **7**, 1888 (1973).
- [4] L. M. Krauss, S. Nasri and M. Trodden, Phys. Rev. D **67**, 085002 (2003) [hep-ph/0210389]; M. Aoki, S. Kanemura and O. Seto, Phys. Rev. Lett. **102**, 051805 (2009) [arXiv:0807.0361 [hep-ph]]; M. Aoki, S. Kanemura and O. Seto, Phys. Rev. D **80**, 033007 (2009) [arXiv:0904.3829 [hep-ph]]; M. Aoki, S. Kanemura, T. Shindou

- and K. Yagyu, JHEP **1007**, 084 (2010) [JHEP **1011**, 049 (2010)] [arXiv:1005.5159 [hep-ph]]; S. Kanemura, O. Seto and T. Shimomura, Phys. Rev. D **84**, 016004 (2011) [arXiv:1101.5713 [hep-ph]]; M. Aoki, S. Kanemura and K. Yagyu, Phys. Lett. B **702**, 355 (2011) [Erratum-ibid. B **706**, 495 (2012)] [arXiv:1105.2075 [hep-ph]]; M. Lindner, D. Schmidt and T. Schwetz, Phys. Lett. B **705**, 324 (2011) [arXiv:1105.4626 [hep-ph]]; S. Kanemura, T. Nabeshima and H. Sugiyama, Phys. Rev. D **85**, 033004 (2012) [arXiv:1111.0599 [hep-ph]]; Y. H. Ahn and H. Okada, Phys. Rev. D **85**, 073010 (2012) [arXiv:1201.4436 [hep-ph]]; S. S. C. Law and K. L. McDonald, Phys. Lett. B **713**, 490 (2012) [arXiv:1204.2529 [hep-ph]]; G. Guo, X. -G. He and G. -N. Li, JHEP **1210**, 044 (2012) [arXiv:1207.6308 [hep-ph]]; P. S. Bhupal Dev and A. Pilaftsis, Phys. Rev. D **87**, 053007 (2013) [arXiv:1212.3808 [hep-ph]]; M. Gustafsson, J. M. No and M. A. Rivera, Phys. Rev. Lett. **110**, no. 21, 211802 (2013) [arXiv:1212.4806 [hep-ph]]; A. Ahriche and S. Nasri, JCAP **1307**, 035 (2013) [arXiv:1304.2055]; A. Ahriche, C. S. Chen, K. L. McDonald and S. Nasri, Phys. Rev. D **90**, 015024 (2014) [arXiv:1404.2696 [hep-ph]]; A. Ahriche, K. L. McDonald and S. Nasri, JHEP **1410**, 167 (2014) [arXiv:1404.5917 [hep-ph]]; C. S. Chen, K. L. McDonald and S. Nasri, Phys. Lett. B **734**, 388 (2014) [arXiv:1404.6033 [hep-ph]].
- [5] M. Aoki, J. Kubo and H. Takano, Phys. Rev. D **87**, 116001 (2013) [arXiv:1302.3936 [hep-ph]]; Y. Kajiyama, H. Okada and K. Yagyu, Nucl. Phys. B **874**, 198 (2013) [arXiv:1303.3463 [hep-ph]]; Y. Kajiyama, H. Okada and T. Toma, Phys. Rev. D **88**, no. 1, 015029 (2013) [arXiv:1303.7356]; S. S. C. Law and K. L. McDonald, JHEP **1309**, 092 (2013) [arXiv:1305.6467 [hep-ph]]; E. Ma, I. Picek and B. Radovic Phys. Lett. B **726**, 744 (2013) [arXiv:1308.5313 [hep-ph]]; D. Restrepo, O. Zapata and C. E. Yaguna, JHEP **1311**, 011 (2013) [arXiv:1308.3655 [hep-ph]]; V. Brdar, I. Picek and B. Radovic, Phys. Lett. B **728**, 198 (2014) [arXiv:1310.3183 [hep-ph]]; H. Okada and K. Yagyu, Phys. Rev. D **89**, no. 5, 053008 (2014) [arXiv:1311.4360 [hep-ph]]; S. Baek, H. Okada and T. Toma, arXiv:1312.3761 [hep-ph]; S. Baek, H. Okada and T. Toma, arXiv:1401.6921 [hep-ph]; H. Okada, arXiv:1404.0280 [hep-ph]; A. Ahriche, C. S. Chen, K. L. McDonald and S. Nasri, Phys. Rev. D **90**, 015024 (2014) [arXiv:1404.2696 [hep-ph]].
- [6] J. N. Ng and A. de la Puente, Phys. Rev. D **90**, no. 9, 095018 (2014) [arXiv:1404.1415 [hep-ph]]; S. Kanemura, T. Matsui and H. Sugiyama, Phys. Rev. D **90**, 013001 (2014) [arXiv:1405.1935 [hep-ph]]; H. Okada and K. Yagyu, Phys. Rev. D **90**, 035019 (2014) [arXiv:1405.2368 [hep-ph]]; S. Kanemura, N. Machida and T. Shindou, Phys. Lett. B **738**, 178 (2014) [arXiv:1405.5834 [hep-ph]]; M. Aoki and T. Toma, JCAP **1409**, 016 (2014) [arXiv:1405.5870 [hep-ph]]; H. Ishida and H. Okada, arXiv:1406.5808 [hep-ph]; H. Okada and Y. Orikasa, Phys. Rev. D **90**, 075023 (2014) [arXiv:1407.2543 [hep-ph]]; H. Okada, T. Toma and K. Yagyu, Phys. Rev. D **90**, 095005 (2014) [arXiv:1408.0961 [hep-ph]]; H. Hatanaka, K. Nishiwaki, H. Okada and Y. Orikasa, arXiv:1412.8664 [hep-ph]; S. Baek, H. Okada and K. Yagyu, arXiv:1501.01530 [hep-ph]; L. G. Jin, R. Tang and F. Zhang, Phys. Lett. B **741**, 163 (2015) [arXiv:1501.02020 [hep-ph]]; H. Okada, arXiv:1503.04557 [hep-ph]; H. Okada, N. Okada and Y. Orikasa, arXiv:1504.01204 [hep-ph].

- [7] P. Culjak, K. Kumericki and I. Picek, Phys. Lett. B **744**, 237 (2015) [arXiv:1502.07887 [hep-ph]]; D. Restrepo, A. Rivera, M. Sanchez-Pelaez, O. Zapata and W. Tangarife, arXiv:1504.07892 [hep-ph]; S. Kashiwase, H. Okada, Y. Orikasa and T. Toma, arXiv:1505.04665 [hep-ph]; M. Aoki, T. Toma and A. Vicente, arXiv:1507.01591 [hep-ph]; K. Nishiwaki, H. Okada and Y. Orikasa, Phys. Rev. D **92**, no. 9, 093013 (2015) [arXiv:1507.02412 [hep-ph]]; W. Wang and Z. L. Han, Phys. Rev. D **92**, 095001 (2015) [arXiv:1508.00706 [hep-ph]]. A. Aranda and E. Peinado, Phys. Lett. B **754**, 11 (2016) [arXiv:1508.01200 [hep-ph]]; A. Ahriche, K. L. McDonald and S. Nasri, Phys. Rev. D **92** (2015) 9, 095020 [arXiv:1508.05881 [hep-ph]]; H. Okada and Y. Orikasa, Phys. Rev. D **93**, no. 1, 013008 (2016) [arXiv:1509.04068 [hep-ph]]; H. Okada and Y. Orikasa, arXiv:1512.06687 [hep-ph]; S. Kanemura, K. Nishiwaki, H. Okada, Y. Orikasa, S. C. Park and R. Watanabe, arXiv:1512.09048 [hep-ph]; T. Nomura, H. Okada and Y. Orikasa, arXiv:1602.08302 [hep-ph]; W. B. Lu and P. H. Gu, arXiv:1603.05074 [hep-ph].
- [8] A. Ahriche, K. L. McDonald, S. Nasri and T. Toma, Phys. Lett. B **746**, 430 (2015) [arXiv:1504.05755 [hep-ph]].
- [9] R. Hempfling, Phys. Lett. B **379**, 153 (1996) [hep-ph/9604278]; K. A. Meissner and H. Nicolai, Phys. Lett. B **648**, 312 (2007) [hep-th/0612165]; W. F. Chang, J. N. Ng and J. M. S. Wu, Phys. Rev. D **75**, 115016 (2007) [hep-ph/0701254 [hep-ph]]; R. Foot, A. Kobakhidze and R. R. Volkas, Phys. Lett. B **655** 156 (2007) [arXiv:0704.1165 [hep-ph]]; T. Hambye and M. H. G. Tytgat, Phys. Lett. B **659**, 651 (2008) [arXiv:0707.0633 [hep-ph]]; R. Foot, A. Kobakhidze, K. L. McDonald and R. R. Volkas, Phys. Rev. D **77**, 035006 (2008) [arXiv:0709.2750 [hep-ph]]; T. Hur and P. Ko, Phys. Rev. Lett. **106**, 141802 (2011) [arXiv:1103.2571 [hep-ph]]; L. Alexander-Nunneley and A. Pilaftsis, JHEP **1009**, 021 (2010) [arXiv:1006.5916 [hep-ph]]; For related recent works see e.g., A. Farzinnia, Phys. Rev. D **92**, no. 9, 095012 (2015) [arXiv:1507.06926 [hep-ph]]; A. D. Plascencia, JHEP **1509**, 026 (2015) [arXiv:1507.04996 [hep-ph]]; K. Hashino, S. Kanemura and Y. Orikasa, Phys. Lett. B **752**, 217 (2016) [arXiv:1508.03245 [hep-ph]]; A. J. Helmboldt, P. Humbert, M. Lindner and J. Smirnov, arXiv:1603.03603 [hep-ph]; K. Allison, C. T. Hill and G. G. Ross, Phys. Lett. B **738**, 191 (2014) [arXiv:1404.6268 [hep-ph]]; P. G. Ferreira, C. T. Hill and G. G. Ross, arXiv:1603.05983 [hep-th]; A. Salvio and A. Strumia, JHEP **1406**, 080 (2014) [arXiv:1403.4226 [hep-ph]]; K. Kannike, G. Htsi, L. Pizza, A. Racioppi, M. Raidal, A. Salvio and A. Strumia, JHEP **1505**, 065 (2015) [arXiv:1502.01334 [astro-ph.CO]].
- [10] R. Foot, A. Kobakhidze, K. L. McDonald and R. R. Volkas, Phys. Rev. D **76** 075014 (2007) [arXiv:0706.1829 [hep-ph]]; S. Iso, N. Okada and Y. Orikasa, Phys. Lett. B **676**, 81 (2009) [arXiv:0902.4050 [hep-ph]]; H. Davoudiasl and I. M. Lewis, Phys. Rev. D **90**, no. 3, 033003 (2014) [arXiv:1404.6260 [hep-ph]]; Z. Kang, Eur. Phys. J. C **75**, no. 10, 471 (2015) [arXiv:1411.2773 [hep-ph]]; H. Okada and Y. Orikasa, arXiv:1412.3616 [hep-ph]; J. Guo, Z. Kang, P. Ko and Y. Orikasa, Phys. Rev. D **91**, no. 11, 115017 (2015) [arXiv:1502.00508 [hep-ph]]; P. Humbert, M. Lindner and J. Smirnov, JHEP **1506**, 035 (2015) [arXiv:1503.03066 [hep-ph]]; P. Humbert, M. Lindner, S. Patra and J. Smirnov, JHEP **1509**, 064 (2015) [arXiv:1505.07453 [hep-ph]]; A. Karam and K. Tamvakis, Phys.

- Rev. D **92**, no. 7, 075010 (2015) [arXiv:1508.03031 [hep-ph]]; H. Okada, Y. Orikasa and K. Yagyu, arXiv:1510.00799 [hep-ph].
- [11] A. Ahriche, K. L. McDonald and S. Nasri, JHEP **1602**, 038 (2016) [arXiv:1508.02607 [hep-ph]].
- [12] J. S. Lee and A. Pilaftsis, Phys. Rev. D **86**, 035004 (2012) [arXiv:1201.4891 [hep-ph]]; M. Lindner, S. Schmidt and J. Smirnov, JHEP **1410**, 177 (2014) [arXiv:1405.6204 [hep-ph]].
- [13] E. Gildener and S. Weinberg, Phys. Rev. D **13**, 3333 (1976).
- [14] A. Ahriche, A. Manning, K. L. McDonald and S. Nasri, arXiv:1604.05995 [hep-ph].
- [15] B. Pontecorvo, Sov. Phys. JETP **26**, 984 (1968) [Zh. Eksp. Teor. Fiz. **53**, 1717 (1967)]; Z. Maki, M. Nakagawa and S. Sakata, Prog. Theor. Phys. **28**, 870 (1962).
- [16] D. V. Forero, M. Tortola and J. W. F. Valle, Phys. Rev. D **86**, 073012 (2012) [arXiv:1205.4018 [hep-ph]].
- [17] J. A. Casas, A. Ibarra, Nucl. Phys. **B618** (2001) 171, hep-ph/0103065.
- [18] P. Bechtle, S. Heinemeyer, O. Stal, T. Stefaniak, and G. Weiglein, JHEP 1411 (2014) 039, [arXiv:1403.1582].
- [19] J. Kubo, E. Ma and D. Suematsu, Phys. Lett. B **642**, 18 (2006) [hep-ph/0604114].
- [20] K. S. Babu and E. Ma, Int. J. Mod. Phys. A **23**, 1813 (2008) [arXiv:0708.3790 [hep-ph]].
- [21] K. Cheung and O. Seto, Phys. Rev. D **69**, 113009 (2004) [hep-ph/0403003].
- [22] A. Ahriche, A. Arhrib and S. Nasri, JHEP02 (2014) 042.
- [23] X.G. He, T. Li, X.Q. Li, J. Tandean and H.C. Tsai, Phys. Rev. D **79** (2009) 023521 (arXiv:0811.0658 [hep-ph]).
- [24] OPAL Collaboration (G. Abbiendi et al.), Eur. Phys. J. C **27** (2003) 311-329.
- [25] R. Foot, A. Kobakhidze, K. L. McDonald and R. R. Volkas, Phys. Rev. D **89**, no. 11, 115018 (2014) [arXiv:1310.0223 [hep-ph]].
- [26] D. S. Akerib *et al.* [LUX Collaboration], arXiv:1310.8214 [astro-ph.CO]; D. S. Akerib *et al.* [LUX Collaboration], arXiv:1512.03506 [astro-ph.CO].